Journal of Alloys and Compounds 507 (2010) 465–469

Contents lists available at ScienceDirect

Journal of Alloys and Compounds

journal homepage: www.elsevier.com/locate/jallcom

Optimization of soft magnetic properties and crystallization in FeAgNbSiB, FeAgNbB and FeAgCoNbB amorphous alloys

Z. Stokłosa[a,*], P. Kwapuliński[a], J. Rasek[a], G. Badura[a], G. Haneczok[a], L. Pająk[a], A. Kolano-Burian[b]

[a] Institute of Materials Science, University of Silesia, Bankowa 12, 40-007 Katowice, Poland
[b] Institute of Non-Ferrous Metals, Sowińskiego 5, 44-100 Gliwice, Poland

ARTICLE INFO

Article history:
Received 1 June 2010
Received in revised form 27 July 2010
Accepted 27 July 2010
Available online 4 August 2010

Keywords:
Amorphous alloys
Optimization effects
Magnetic measurements

ABSTRACT

In the present paper the influence of 1-h annealing (temperature range from 300 to 800 K) on magnetic, plastic and electrical properties of the $Fe_{75.75}Ag_{0.25}Nb_2Si_{13}B_9$, $Fe_{75.75}Ag_{0.25}Nb_2B_{22}$, $Fe_{74.75}Ag_{0.25}Co_5Nb_2B_{18}$ amorphous alloys were carefully examined. For all the tested alloys the enhancement of magnetic permeability effect was observed—i.e. initial magnetic permeability measured at room temperature for annealed samples shows a sharp maximum. A possible mechanism explaining this effect is discussed in detail. Moreover it was found that at room temperature plastic deformation of the annealed samples depends on the progress of structural relaxation (free volume content). Activation energies and preexponential factors of the first stage of crystallization process were determined from the isochronal resistivity curves measured with different heating rates (Kissinger method). The Curie temperatures from the magnetization curves versus temperature were also determined.

1. Introduction

Amorphous alloys based on iron obtained by melt spinning technique belong to modern soft magnetic materials. Because of some unique properties (very high magnetic permeability and also resistivity) these alloys have found nowadays industrial applications in the field of electrical engineering as magnet cores or different kind of sensors [1–5]. Moreover magnetic properties of amorphous alloys based on iron can be significantly improved by applying a specific thermal annealing [6–9]. The conditions of the so-called optimization annealing (i.e. temperature and time) strongly depend on alloying additions and free volume content frozen into material during fabrication. For many alloys the optimization effect is explained by formation of a nanocrystalline phase, i.e. formation of iron nanograins embedded into amorphous surroundings. Such a microstructure averages out magnetic anisotropy and gives the enhancement of magnetic permeability effect [10–13]. Some alloying additions (like 1 at% of Cu and 2–3 at% high-melting elements) make easer formation of the nanocrystalline phase and from this point of view the efficiency of the optimization annealing is still under examinations. Nowadays, in literature three different groups of amorphous and nanocrystalline alloys are considered: FINEMET (Fe–Cu–Nb–Si–B [14]), NANOPERM (Fe–Cu–Nb–Zr–Hf-B [15]) and HITPERM (FeCoCuZr–Nb–Hf-B [16–18]). It is proper to add that the main disadvantage of the nanocrystalline magnets consists in material brittleness. In fact, formation of a large number of iron nanograins into amorphous matrix causes a considerable increase of brittleness in relation to the as quenched state. Therefore examination of embrittlement for example via measuring the deformation corresponding to formation of bending cracks seems to be especially important [19,20].

Material brittleness of the annealed amorphous alloys can be reduced by applying special alloying additions causing the enhancement of magnetic permeability without formation of a nanocrystalline phase. Indeed as it was shown in [21–27] a significant increase of permeability observed in samples free of iron nanograins was attributed to annealing out of free volume and a reduction of internal stresses, i.e. to the so-called relaxed amorphous phase.

The aim of the present paper is to examine the influence of small addition of silver atoms (0.25 at% ≈ 0.50 wt% in the $Fe_{75.75}Ag_{0.25}Nb_2Si_{13}B_9$, $Fe_{75.75}Ag_{0.25}Nb_2B_{22}$, and $Fe_{74.75}Ag_{0.25}Co_5Nb_2B_{18}$ amorphous alloys) on crystallization processes and plastic properties of the examined material in the context of the optimization of soft magnetic properties effect.

2. Material and experimental procedure

Experiments were carried out for the $Fe_{75.75}Ag_{0.25}Nb_2Si_{13}B_9$, $Fe_{75.75}Ag_{0.25}Nb_2B_{22}$ and $Fe_{74.75}Ag_{0.25}Co_5Nb_2B_{18}$ amorphous alloys obtained by melt spinning technique in the form of strips with thickness and width of about 20 μm and 10 mm, respectively. The samples were annealed in the vacuum for 1 h at temperatures T_a ranging from 300 to 800 K (step 25 K) and at room temperature the following properties were measured: (i) magnetization curves $B = B(H)$ and permeability versus magnetic

* Corresponding author. Tel.: +48 32 3591554; fax: +48 32 2596929.
E-mail address: stoklosa@us.edu.pl (Z. Stokłosa).

0925-8388/$ – see front matter © 2010 Elsevier B.V. All rights reserved.
doi:10.1016/j.jallcom.2010.07.205

field curves $\mu_r = \mu_r(H)$ (Lake Shore fluxmeter), (ii) parallel magnetostriction coefficient at saturation magnetic field $\lambda_{s||}$ (dilatometer with infrared detector), (iii) initial magnetic permeability and magnetic relaxation $\Delta\mu/\mu = f(T_a)$ ($\Delta\mu = \mu(t_1) - \mu(t_2)$ for $t_1 = 0.5$ min, $t_2 = 30$ min after demagnetization, field 0.5 A/m, RLC meter of type HP 4284A), (iv) saturation magnetic polarization at temperature 10 K and 300 K (magnetic induction 7 T, PPMS Quantum Design), (v) electrical resistivity (four point probe), (vi) deformation corresponding to formation of bending cracks calculated as: $\varepsilon = d/2r$ (where d is the sample thickness and r is the bending radius) [19,20].

Crystallization kinetics was examined by applying "in situ" measurements of electrical resistivity versus temperature with different heating rates (0.5–10 K/min). Based on this kind of measurement activation energies and preexponential factors of the first stage of crystallization were calculated using the Kissinger method [28]. The Curie temperature of amorphous phase and also the crystallization temperatures of the alloys examined were also determined by applying measurements of magnetization in saturation versus temperature (magnetic balance, temperature range 300–1100 K, magnetic induction 0.5 T, heating rate 5 K/min).

Structural changes in annealed samples were examined by applying X-ray diffractometer X'Pert PW 304060 and high resolution transmission electron microscope (HREM) Jeol 3010 B.

3. Results

All the alloys examined in the as quenched state were amorphous which is documented in Fig. 1 where an example of HREM image and the corresponding electron diffraction pattern for $Fe_{75.75}Ag_{0.25}Nb_2B_{22}$ alloy are shown.

Fig. 2 shows three curves of the normalized magnetization in saturation $M(T)/M(300\,K)$ versus absolute temperature T obtained for the $Fe_{75.75}Ag_{0.25}Nb_2Si_{13}B_9$, $Fe_{75.75}Ag_{0.25}Nb_2B_{22}$ and $Fe_{74.75}Ag_{0.25}Co_5Nb_2B_{18}$ alloys in the as quenched state (heating rate 5 K/min, magnetic induction 0.5 T). In this figure one can distinguish four different temperature ranges of magnetization change. In the first region, let say "a", the magnetization monotonically decreases with temperature up to the Curie point of the amorphous phase T_c. The determined values of T_c (inflection point of magnetization curve in the region "a") are the following: 626 K, 636 K and 638 K for the $Fe_{75.75}Ag_{0.25}Nb_2Si_{13}B_9$, $Fe_{75.75}Ag_{0.25}Nb_2B_{22}$ and $Fe_{74.75}Ag_{0.25}Co_5Nb_2B_{18}$ alloys, respectively. At $T > T_c$, let say in the region "b", the examined alloys are in paramagnetic state and at higher temperatures (region "c") an increase of the magnetization due to formation of αFe nanocrystallities (nanocrystalline phase) is observed. The determined temperatures of nanocrystallization (inflection point of magnetization curve in the region "c"; heating rate 5 K/min) are the following: 820 K, 790 K and 725 K for the $Fe_{75.75}Ag_{0.25}Nb_2Si_{13}B_9$, $Fe_{75.75}Ag_{0.25}Nb_2B_{22}$ and $Fe_{74.75}Ag_{0.25}Co_5Nb_2B_{18}$ alloys, respectively. It is obvious that in the region "d" magnetization changes correspond to the crystalline phase.

Fig. 3 shows isochronal resistivity curves $\rho(T)$ measured with heating rate 0.5 K/min for all alloys examined. Initially, the resistivity slightly increases with temperature due to scattering of conduction electrons by phonons of amorphous lattice. The temperature coefficients of resistivity α determined from these curves at 300 K are $7.2 \times 10^{-5}\,K^{-1}$, $7.0 \times 10^{-5}\,K^{-1}$, and $7.4 \times 10^{-5}\,K^{-1}$ for the $Fe_{75.75}Ag_{0.25}Nb_2Si_{13}B_9$, $Fe_{75.75}Ag_{0.25}Nb_2B_{22}$ and $Fe_{74.75}Ag_{0.25}Co_5Nb_2B_{18}$ alloys, respectively. The crystallization (nanocrystallization) of amorphous structure is observed at higher temperatures as a sharp drop of resistivity. The crystallization temperatures determine from the condition $d\rho/dT = 0$ are the following 780 K, 742 K and 670 K for the same sequence of the examined alloys. Activation energies E_{x1} and preexponential factors K_{01} of the first stage of crystallization process (formation of αFe nanograins) were determined based on the resistivity curves measured with different heating rates (0.5–10 K/min) and the Kissinger approach [25]. The obtained values are $E_{x1} = 3.3$ eV and $K_{01} = 8.2 \times 10^{16}\,s^{-1}$, $E_{x1} = 3.1$ eV and $K_{01} = 2.73 \times 10^{16}\,s^{-1}$, $E_{x1} = 2.8$ eV and $K_{01} = 1.42 \times 10^{16}\,s^{-1}$.

Fig. 4 shows initial magnetic permeability measured at room temperature (field 0.5 A/m, frequency about 1 kHz) versus tem-

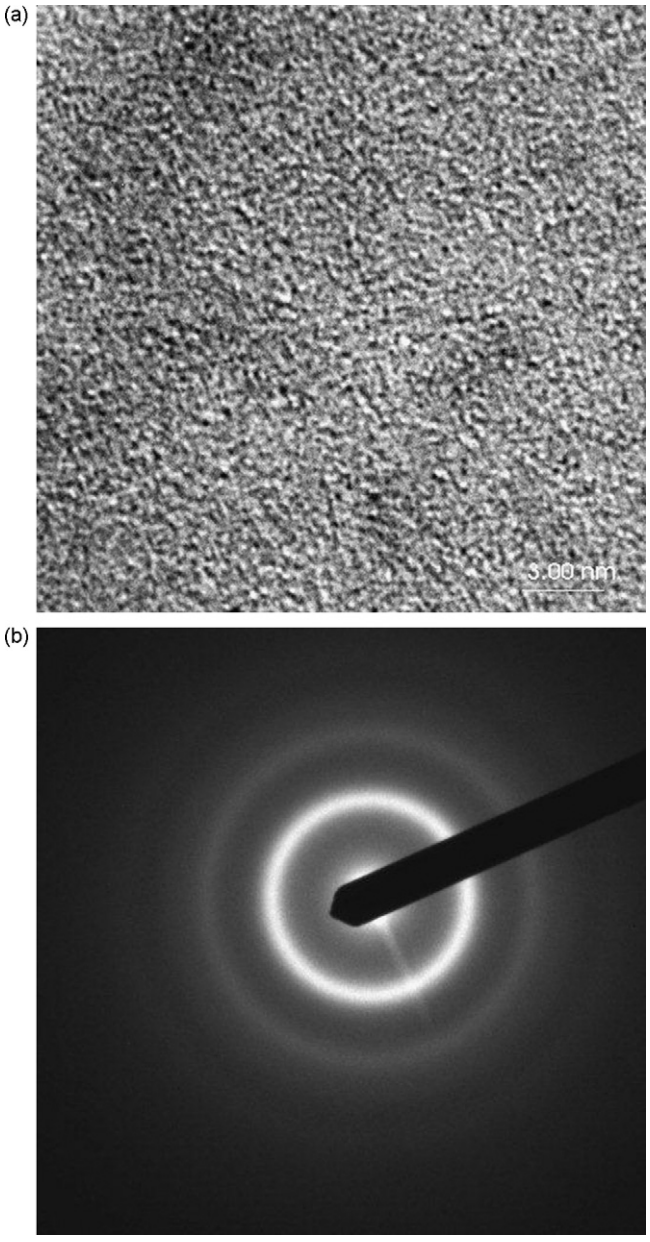

Fig. 1. HREM image (a) and the corresponding electron diffraction pattern (b) for $Fe_{75.75}Ag_{0.25}Nb_2B_{22}$ alloy in the as quenched state.

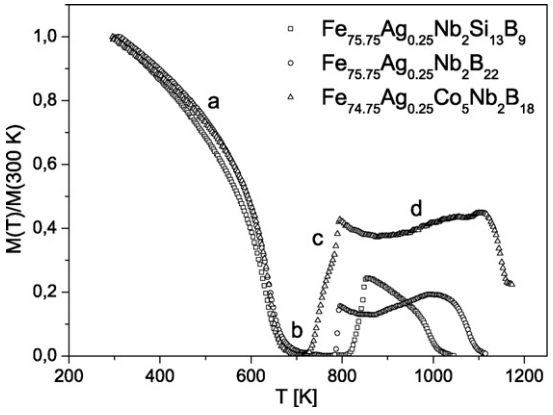

Fig. 2. Normalized magnetization versus absolute temperature for all alloys examined (heating rate $v = 5$ K/min; different temperature ranges are denoted as "a", "b", "c", and "d" (see the text)).

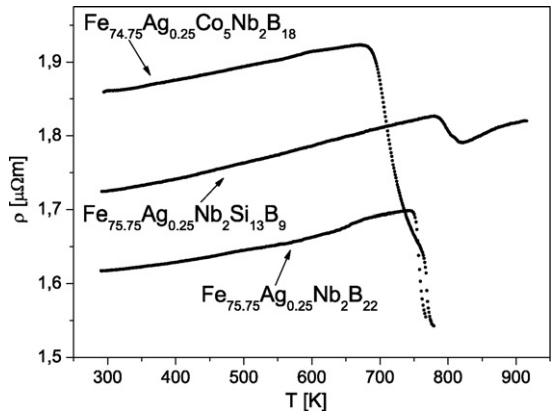

Fig. 3. Electrical resistivity versus absolute temperature for all alloys examined (heating rate $v = 0.5$ K/min).

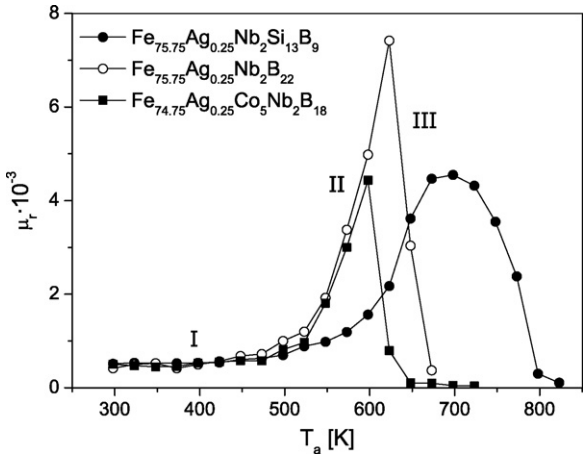

Fig. 4. Initial relative magnetic permeability (field 0.5 A/m) μ_r measured at room temperature versus the 1-h annealing temperature T_a for all alloys examined.

perature of 1-h preliminary annealing T_a. As it can be seen in all cases the curves $\mu_r = \mu_r(T_a)$ shows a distinct maximum at temperature T_{op} being per definition the 1-h optimization annealing temperature. Careful examinations of microstructure of the optimized samples (annealed at T_{op}) carried out by applying X-ray diffraction and high resolution electron microscopy do not show any traces of nanostructure. This is documented in Fig. 5, where

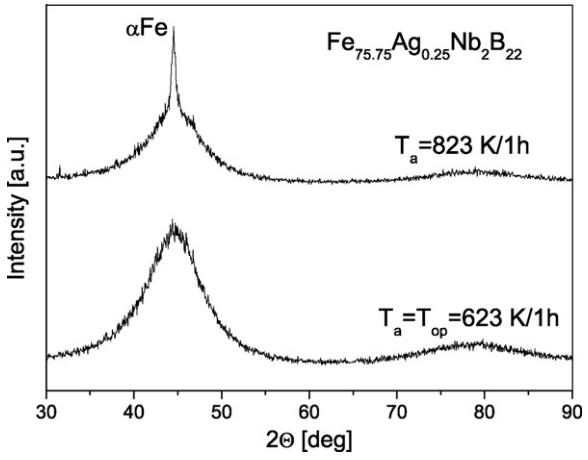

Fig. 5. X-ray spectra obtained for $Fe_{75.75}Ag_{0.25}Nb_2B_{22}$ alloy annealed at $T_a = T_{op} = 623$ K/1 h and at $T_a = 823$ K/1 h.

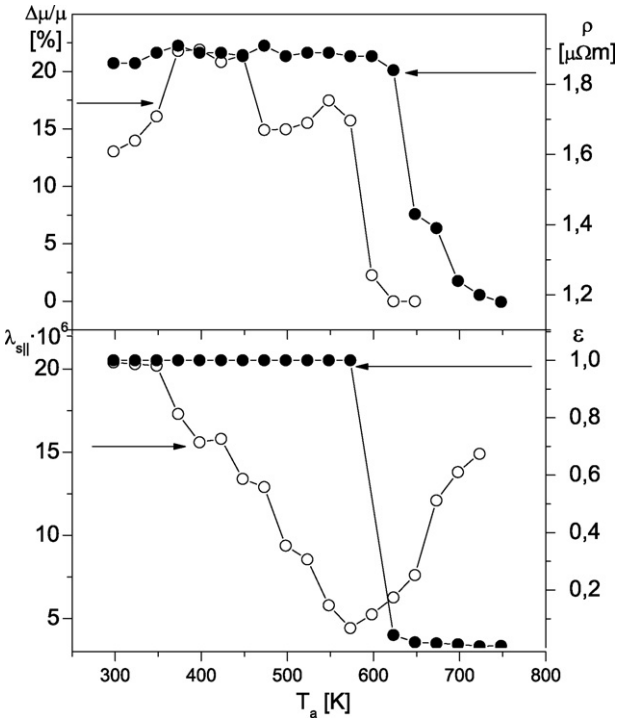

Fig. 6. Parallel magnetostriction ($\lambda_{s||}$), intensity of magnetic relaxation ($\Delta\mu/\mu$), electrical resistivity (ρ) and deformation corresponding to formation of bending cracks (ε) measured at room temperature versus the 1-h annealing temperature T_a for the $Fe_{74.75}Ag_{0.25}Co_5Nb_2B_{18}$ alloy.

X-ray spectra obtained for $Fe_{75.75}Ag_{0.25}Nb_2B_{22}$ alloy annealed at $T_a = T_{op} = 623$ K/1 h and at $T_a = 823$ K/1 h are presented.

In order to find a proper mechanism describing the optimization effect (presented in Fig. 4) additional examination were performed, i.e. for annealed samples magnetic relaxation $\Delta\mu/\mu = f(T_a)$, parallel magnetostriction coefficient $\lambda_{s||} = f(T_a)$, deformation corresponding to formation of bending cracks $\varepsilon = \varepsilon(T_a)$ and resistivity $\rho = \rho(T_a)$ were measured. For example the obtained results for the $Fe_{74.75}Ag_{0.25}Co_5Nb_2B_{18}$ alloy are presented in Fig. 6. Regardless of some detail, one can see that $\Delta\mu/\mu$, ρ and ε decrease with increasing annealing temperature at least for $600\text{ K} < T_a < T_{op}$ K. In contrast to this $\lambda_{s||}$ significantly decreases starting from $T_a = 350$ K.

4. Discussion

It is known that silver atoms do not posses magnetic moment [29] and from this reason one can expect that in the examined alloys the Curie temperature should be lower in relation to silver free alloys. Indeed, such a conclusion is confirmed by our results. Comparing the Curie temperature for the $Fe_{75.75}Ag_{0.25}Nb_2Si_{13}B_9$, $Fe_{75.75}Ag_{0.25}Nb_2B_{22}$ amorphous alloys with T_c of the $Fe_{76}Nb_2Si_{13}B_9$ and $Fe_{76}Nb_2B_{22}$ amorphous alloys studied in [23,30] one can conclude that the presence of silver causes a decrease of T_c by about 10 and 14 K, respectively. Taking into account the alloys $Fe_{80}Nb_2B_{18}$ studied in [30] and the $Fe_{74.75}Ag_{0.25}Co_5Nb_2B_{18}$ alloy one can conclude that Co atoms causes an increase of the Curie temperature. It is proper to add that boron atoms play similar role on value of T_c as it was discussed in [30], i.e. increase of T_c with increase of B concentration.

Boron atoms with relatively small atomic radius (81 pm) in relation to the radius of Fe atoms (124 pm) cause an increase of Fe–Fe distances [31]. According to the Bethe–Slater graph the exchange energy can increase with increasing interatomic distances [32] and it leads to an increase of the Curie temperature.

Table 1
The Curie temperatures T_c, the temperatures of the first stage of crystallization T_{x1} ($v = 5$ K/min), activation energies and preexponential factors of the first stage of crystallization process (E_{x1}, K_{01}), the temperature of the 1-h optimization annealing T_{op}, electrical resistivity at 300 K (ρ_{300}), temperature coefficients of resistivity α determined at 300 K (α_{300}), saturation magnetic polarization in the as quenched state at 300 K and 10 K (J_{300} and J_{10}), initial magnetic permeability in the as quenched state μ_r^{asq} and after optimization annealing at T_{op} μ_r^{opt}, the parallel magnetostriction coefficients $\lambda_{s\|}^{asq}$ (and $\lambda_{s\|}^{opt}$), the intensity of magnetic relaxation $(\Delta\mu/\mu)^{asq}$ (and $(\Delta\mu/\mu)^{opt}$), deformation corresponding to formation of bending cracks ε^{asq} (and ε^{opt}).

Physical quantity	Material		
	$Fe_{75.75}Ag_{0.25}Nb_2Si_{13}B_9$	$Fe_{75.75}Ag_{0.25}Nb_2B_{22}$	$Fe_{74.75}Ag_{0.25}Co_5Nb_2B_{18}$
T_c [K]	626	636	638
T_{x1} [K]	820	790	725
T_{op} [K]	698	623	598
E_{x1} [eV]	3.3	3.1	2.8
K_{01} [$\times 10^{16}$ s^{-1}]	8.2	2.7	1.4
$\rho_{300\,K}$ [$\times 10^{-8}$ Ωm]	172	162	186
$\alpha_{300\,K}$ [$\times 10^{-5}$ K^{-1}]	7.2	7.0	7.4
$\lambda_s^{asq} \times 10^6$	17.7	12.4	20.4
$\lambda_s^{opt} \times 10^6$	2.0	2.8	5.2
J_{300} [T]	1.22	1.28	1.10
J_{10} [T]	1.40	1.47	1.13
$(\Delta\mu/\mu)^{asq}$ [%]	8.1	16.7	13.0
$(\Delta\mu/\mu)^{opt}$ [%]	4.9	1.4	2.3
ε^{asq}	0.0583	1	1
ε^{opt}	0.0181	0.0153	0.0927
μ_r^{asq}	510	420	500
μ_r^{opt}	4550	7400	4430

The influence of silver atoms on the temperature of the first stage of crystallization is similar which also was discussed in [33,34] for FeAgSiB alloys. For example T_{x1} for the $Fe_{75.75}Ag_{0.25}Nb_2Si_{13}B_9$ alloy in relation to the $Fe_{76}Nb_2Si_{13}B_9$ alloy [23] is lower by about 40 K.

The material characteristic determined in the present paper, i.e. the Curie temperatures T_c, the temperatures of the first stage of crystallization T_{x1} ($v = 5$ K/min), activation energies and preexponential factors of the first stage of crystallization process (E_{x1}, K_{01}), the temperature of the 1-h optimization annealing T_{op}, electrical resistivity at 300 K (ρ_{300}), temperature coefficients of resistivity α determined at 300 K (α_{300}), saturation magnetic polarization in the as quenched state at 300 K and 10 K (J_{300} and J_{10}), initial magnetic permeability in the as quenched state μ_r^{asq} and after optimization annealing at T_{op} μ_r^{opt}, the parallel magnetostriction coefficients $\lambda_{s\|}^{asq}$ (and $\lambda_{s\|}^{opt}$), the intensity of magnetic relaxation $(\Delta\mu/\mu)^{asq}$ (and $(\Delta\mu/\mu)^{opt}$), and finally the deformation corresponding to formation of bending cracks ε^{asq} (and ε^{opt}) are presented in Table 1.

The results presented in Fig. 3 show different behavior of the examined alloys during heating. Indeed, the $Fe_{75.75}Ag_{0.25}Nb_2Si_{13}B_9$ alloy crystallizes at higher temperature which can be explained by the presence of Si atoms with higher atomic radius (118 pm) than B atoms.

From this table and Fig. 4 one can conclude that initial magnetic permeability for the examined alloys significantly increases after the optimization annealing. Indeed, the ratio μ_r^{opt}/μ_r^{asq} is about 9, 15 and 9 for the $Fe_{75.75}Ag_{0.25}Nb_2Si_{13}B_9$, $Fe_{75.75}Ag_{0.25}Nb_2B_{22}$ and $Fe_{74.75}Ag_{0.25}Co_5Nb_2B_{18}$ alloy, respectively. It was already mentioned that this effect cannot be explained via formation of a nanocrystalline phase because such a phase was not detected in the optimized samples (X-ray diffraction and high resolution electron microscopy techniques). For this reason the observed changes of magnetic properties should be attributed to the relaxed amorphous phase.

In literature in the context of the optimization effect, three different mechanisms are discussed. The first is related to the decrease of the magnetoelastic energy due to a decrease of the magnetostriction coefficient and stress. In our case (see Table 1) $\lambda_{s\|}^{asq} > \lambda_{s\|}^{opt}$) for all examined alloys. The second mechanism of the enhancement of magnetic permeability effect is related to the so-called stabilization energy describing the interaction of structural defects with the magnetization vector within the magnetic domain. Such defects in amorphous structure, according to Kronmüller, consist of atomic pairs in the vicinity of free volume [35].

The presence of high free volume (high concentration of microvoids) in melt spinning metals can be explained based on the melting model of metals, e.g. [36].

Annealing out of free volume leads to a reduction of stabilization energy and to increase of permeability. From Table 1 one can see that for all examined alloys $(\Delta\mu/\mu)^{asq} > (\Delta\mu/\mu)^{opt}$ which mean that annealing at temperatures $T_a \leq T_{op}$ leads to a reduction of free volume content [23,25]. The third mechanism causing the enhancement of magnetic permeability lies in increase of magnetic polarization due to annealing at the temperature T_{op} [23,37].

Annealing out of free volume is also correlated with the deformation corresponding to formation bending cracks. Indeed, from Fig. 6 and Table 1 one can see that annealing at higher temperatures ($T_a > 650$ K) causes an increase of material brittleness. Comparing isochronal curves related to a change of free volume content, i.e. $\Delta\mu/\mu = f(T_a)$ and $\varepsilon = \varepsilon(T_a)$ one can conclude that embrittlement of amorphous alloys increases with decreasing free volume content. From this point of view free volume in amorphous materials plays similar role as dislocations in crystalline materials.

In the system Fe–Si–B–Nb_2 the addition of $Ag_{0.25}$ causes an increase of the temperature T_{op} in relation to the system Fe–Nb_2–Si–B [38]. On the contrary, for the $FeNb_2B_{22}$ and $FeNb_2Co_5B_{18}$ alloys such increase is not observed.

Silver atoms show relatively weak solubility in iron and from this reason some nucleation centers for precipitation of αFe(Si) crystalline phase can be formed easily. However, Nb atoms with high atomic radius (208 pm) cause a slowing down of diffusion processes and what follows make the growth of αFe(Si) crystallites more difficult.

5. Conclusions

The main conclusions from his paper can be summarized as follows:

- In the examined alloys due to the enhancement of soft magnetic properties effect (1-h annealing at temperatures T_{op} listed in Table 1) permeability increases about 9, 15 and 9 times in

relation to the as quenched state for the $Fe_{75.75}Ag_{0.25}Nb_2Si_{13}B_9$, $Fe_{75.75}Ag_{0.25}Nb_2B_{22}$ and $Fe_{74.75}Ag_{0.25}Co_5Nb_2B_{18}$ alloys, respectively.

- Silver atoms as an alloying additions cause a decrease of the Curie temperature of amorphous phase.
- Silver atoms as an alloying additions cause a decrease of the temperature of the first stage of crystallization.
- Embrittlement of the examined alloys measured as a deformation corresponding to formation of bending cracks increases with decreasing of free volume content.

Acknowledgments

This work was supported by the Polish Ministry of Science and High School under grant No. NN 507460633.

References

[1] M.E. Mc Henry, D.E. Laughlin, Acta Mater. 48 (2000) 223–238.
[2] S.H. Al-Heniti, J. Alloys Compd. 484 (2009) 177–184.
[3] R. Sahingoz, M. Erol, M.R.J. Gibbs, J. Magn. Magn. Mater. 271 (2004) 74–78.
[4] R. Hasegawa, J. Magn. Magn. Mater. 215–216 (2000) 240–245.
[5] M. Ohta, Y. Yoshizawa, J. Magn. Magn. Mater. 321 (2009) 2220–2224.
[6] G. Herzer, Handbook of Magnetic Materials, vol. 10, Elsevier Science B.V, Amsterdam, 1997, p. 415.
[7] G. Badura, J. Rasek, P. Kwapuliński, Z. Stokłosa, L. Pająk, Phys. Status Solidi (a) 203 (2006) 349–357.
[8] Z. Stokłosa, J. Rasek, P. Kwapuliński, G. Badura, G. Haneczok, J. Magn. Magn. Mater. 304 (2006) e700–e702.
[9] Ł. Madej, G. Haneczok, A. Chrobak, P. Kwapulinski, Z. Stokłosa, J. Rasek, J. Magn. Magn. Mater. 320 (2008) e774–e777.
[10] T. Kulik, J. Non-Cryst. Sol. 287 (2001) 145–161.
[11] G. Herzer, L.L. Varga, J. Magn. Magn. Mater. 215–216 (2000) 506–512.
[12] G. Herzer, J. Magn. Magn. Mater. 294 (2005) 99–106.
[13] G. Haneczok, J. Rasek, Defect Diffus. Forum 224–225 (2004) 13–26.
[14] Y. Yoshizawa, S. Oguma, K. Yamauchi, J. Appl. Phys. 64 (1988) 6044–6046.
[15] A. Makino, T. Hatanai, Y. Naitoh, T. Bitoh, A. Inoue, IEEE Trans. Magn. 33 (1997) 3793–3798.
[16] X. Liang, T. Kulik, J. Ferenc, B. Xu, J. Magn. Magn. Mater. 308 (2007) 227–232.
[17] J. Zbroszczyk, A. Młynczyk, J. Olszewski, W. Ciurzyńska, M. Hasiak, R. Kolano, J. Lelątko, J. Magn. Magn. Mater. 304 (2006) e727–e729.
[18] R. Hasegawa, J. Magn. Magn. Mater. 304 (2006) 187–191.
[19] H. Chiriac, C. Hison, J. Magn. Magn. Mater. 254–255 (2003) 475–476.
[20] G. Kumar, M. Oknuma, T. Furubashi, T. Ohkubo, K. Hono, J. Non-Crystal. Solids 354 (2008) 882–888.
[21] T. Naohara, Philos. Mag. Lett. 78 (1998) 229–234.
[22] T. Naohara, Philos. Mag. Lett. 78 (1998) 235–239.
[23] G. Badura, J. Rasek, Z. Stokłosa, P. Kwapuliński, G. Haneczok, J. Lelątko, L. Pająk, J. Alloys Compd. 436 (2007) 43–50.
[24] P. Kwapulinski, Z. Stoklosa, J. Rasek, G. Badura, G. Haneczok, L. Pajak, J. Lelatko, J. Magn. Magn. Mater. 320 (2008) e778–e782.
[25] G. Haneczok, J.E. Frąckowiak, A. Chrobak, P. Kwapuliński, J. Rasek, Phys. Status Solidi (a) 202 (2005) 2574–2581.
[26] P. Kwapuliński, L. Pająk, J. Lelątko, G. Badura, J. Rasek, Z. Stokłosa, G. Haneczok, Solid State Phenom. 163 (2010) 225–228.
[27] A. Chrobak, G. Haneczok, Z. Stokłosa, P. Kwapuliński, J. Rasek, G. Chełkowska, Phys. Status Solidi (a) 196 (2003) 248–251.
[28] F. Liu, X.N. Liu, O. Wang, J. Alloys Compd. 473 (2009) 152–156.
[29] A.H. Morrish, The Physical Principles of Magnetism, John Wiley and Sons Inc., New York, 2001.
[30] Z. Stokłosa, J. Rasek, P. Kwapuliński, G. Haneczok, A. Chrobak, J. Lelątko, L. Pająk, Phys. Status Solidi (a) 207 (2010) 452–456.
[31] G.A. Stergioudis, G. Vourlias, H. Morawiec, D. Stróż, E.K. Polychroniadis, Mater. Res. Bull. 39 (2004) 231.
[32] G. Bihlmayer, in: H. Kronmüller, S. Parkin (Eds.), Handbook of Magnetism and Advanced Magnetic Materials, vol. 3, Wiley, Hoboken, 2007.
[33] K. Chrissafis, Thermochim. Acta 411 (2004) 7–11.
[34] K.G. Efthimiadis, S.C. Chadjivasiliou, G. Melidis, J.A. Tsoukalas, J. Mater. Sci. 35 (2000) 2525–2528.
[35] H. Kronmüller, Philos. Mag. B 48 (1983) 127–150.
[36] Q.S. Mei, K. Lu, Prog. Mater. Sci. 52 (2007) 1175–1265.
[37] J. Rasek, Z. Stokłosa, Eng. Trans. 54 (2006) 51–69, Polish Academy of Science, Institute of Fundamental Technological Research.
[38] Z. Stokłosa, G. Badura, P. Kwapuliński, J. Rasek, G. Haneczok, J. Lelątko, L. Pająk, Solid State Phemon. 130 (2007) 171–174.